Biosensors and Bioelectronics 54 (2014) 331–338

Contents lists available at ScienceDirect

Biosensors and Bioelectronics

journal homepage: www.elsevier.com/locate/bios

Quantum dots sensitized titanium dioxide decorated reduced graphene oxide for visible light excited photoelectrochemical biosensing at a low potential

Xianxiang Zeng, Jianchun Bao, Min Han, Wenwen Tu*, Zhihui Dai*

Jiangsu Collaborative Innovation Center of Biomedical Functional Materials and Jiangsu Key Laboratory of Biofunctional Materials, College of Chemistry and Materials Science, Nanjing Normal University, Nanjing 210023, PR China

ARTICLE INFO

Article history:
Received 10 September 2013
Received in revised form
26 October 2013
Accepted 28 October 2013
Available online 4 November 2013

Keywords:
Biosensing
Photoelectrochemistry
Signal amplification
Quantum dots
Reduced graphene oxide

ABSTRACT

A low potential and competitive photoelectrochemical biosensing platform was developed using quantum dots sensitized titanium dioxide decorated reduced graphene oxide (TiO_2–RGO) nanocomposites. The nanocomposites were prepared through electrostatic interaction between mercaptoacetic acid wrapped CdSe quantum dots with negative charge and TiO_2–RGO hybrids with positive charge obtained via ultrasonic and acid treatments. Electron microscopes and spectroscopes were used to characterize the functionalized nanocomposites films of CdSe/TiO_2–RGO, and the fabrication process of the photoelectrochemical biosensor. Based on the high photovoltaic conversion efficiency of CdSe/TiO_2–RGO nanocomposites films, after introducing biological recognition and competitive immunoreaction, a low potential and competitive photoelectrochemical biosensor for carcinoembryonic antigen (CEA) detection was fabricated. The synergic effect of horseradish peroxide and benzo-4-chlorohexadienone decreased the background signal, leading to signal amplification. Under the light irradiation of 430 nm and the applied potential of 0 V, the biosensor detected CEA with a linear range from 0.003 to 100 ng mL^{-1} and the detection limit was estimated to be 1.38 pg mL^{-1} at a *S*/*N* of 3. It was satisfactory for clinical sample detection. The proposed competitive and low potential photoelectrochemical biosensor under irradiation of visible light exhibited good performance, which has a promising prospect in clinical diagnose.

1. Introduction

Compared with conventional detection methods for cancer biomarkers, such as enzyme-linked immunosorbent assay (Ocvirk et al., 2009), radioimmunoassay (Schaefer et al., 2005), piezoelectricity (Zhang et al., 2007), surface plasmon resonance (SPR) (Hu et al., 2010), electrochemistry (Tang and Ren, 2008; Akter et al., 2012; Ho et al., 2009; Zhuo et al., 2009; Nie et al., 2009; Munge et al., 2011; Chikkaveeraiah et al., 2012), chemiluminesce (CL) (Yang et al., 2009) and electrochemiluminescence (ECL) (Ge et al., 2012; Jie et al., 2010; Li et al., 2011a, 2011b), a newly developed photoelectrochemical determination strategy is of special interest for its potential in bioassay (Gill et al., 2008; Chen et al., 2010; Zhang et al., 2011; Tu et al., 2012; Zhao et al., 2012a, 2012b). It avoids drawbacks of expensive equipments, operation at harsh conditions, time-consuming, and difficult for *in situ* or online monitoring, which plays an important role in clinical diagnose for improving long term survival of cancer patient (Kulasingam and Diamandis, 2008). In addition, it also owns the advantages of both optical methods and electrochemical sensors (Ikeda et al., 2009). By using light as the external stimulus at an appropriate wavelength, a selective photoelectrochemical reaction can be achieved. The complete separation of excitation source (light) and detection signal (current) can greatly reduce the undesired background signal. The photoelectrochemical measurement that uses a photocurrent as a detection signal can operate at a low applied potential, and exhibit high sensitivity together with repeating cycles (Wang et al., 2009).

The poor light-response of nanostructured TiO_2 which is caused by its large band gap, limits its application in visible light region (Tang et al., 2010; Lee et al., 2012; Long et al., 2012; Li et al., 2012; Huang et al., 2013). Two possible strategies can be adopted to enhance the photovoltaic conversion efficiency of TiO_2: incorporation of nanoscale carbon materials (Long et al., 2012) and modification of TiO_2 with narrow-band gap semiconductors (Tvrdy et al., 2011; Cai et al., 2013). Reduced graphene oxide (RGO) is a promising material for constructing high performance photovoltaic devices (Tang et al., 2010). When hybridized with other materials, graphene can slow the recombination of photo- or electro-chemically generated electron–hole pairs, increasing

* Corresponding authors. Tel./fax: +86 25 85891051.
E-mail addresses: daizhihuii@njnu.edu.cn, wwt@njnu.edu.cn (Z. Dai).

0956-5663/$ - see front matter © 2013 Elsevier B.V. All rights reserved.
http://dx.doi.org/10.1016/j.bios.2013.10.057

charge transfer rate of electrons and surface-adsorbed amount of chemical molecules through π–π interactions (Lee et al., 2012). Quantum dots (QDs) are active in wide visible range. Therefore, they are promising materials for applications in photodetectors, solar cells, and biosensors (Zhao et al., 2012a, 2012b). Many works have been done to enhance the photovoltaic conversion efficiency of TiO_2 by modification with either QDs (Hensel et al., 2010; Tvrdy et al., 2011) or RGO (Tang et al., 2010; Lee et al., 2012). For the works of QDs sensitized TiO_2 (CdSe/TiO_2) (Hensel et al., 2010; Tvrdy et al., 2011), they mainly solved the problem of narrow sunlight absorption and electron transfer between QDs and TiO_2, while the electron transfer between CdSe/TiO_2 and electrode was restricted and had not been settled. Correspondingly, the implanted graphene sheets in TiO_2–RGO were served as the electron acceptor and transporter for effective charge separation, and rapid transportation of the photogenerated electrons to the electrode. Related works (Tang et al., 2010; Lee et al., 2012) had been reported, however, the narrow absorption in ultraviolet range limited their usages in biomolecules detection. In this work, CdSe/TiO_2–RGO nanocomposites solved the problems of electron–hole recombination, narrow sunlight absorption range in TiO_2, interfacial electron transfer among CdSe, TiO_2 and RGO, and electron transfer between CdSe/TiO_2–RGO nanocomposites and electrodes, which previous researches only resolved one aspect. Meanwhile, the CdSe/TiO_2–RGO nanocomposites with high photovoltaic conversion efficiency have not been applied to photoelectrochemical biosensing yet. Herein, CdSe/TiO_2–RGO nanocomposites films were prepared through layer-by-layer electrostatic assembly, which was a simple, yet elegant method providing nanometer thickness control for a variety of thin-film architectures on various surfaces. The assembly method preferred to fully utilize the sunlight over monolayered QDs obtained by *in situ* preparation (Choi et al., 2012). Noteworthily, this electrostatic interaction assembly increased the amount of CdSe QDs immobilized compared to physical absorption, leading to loading more proteins. Furthermore, after acid treatment, pH-induced protonation of surface groups on TiO_2 nanoparticles tuned the band edge of TiO_2 nanoparticles, which generated an energy gap for facilitating charge injection between excited CdSe QDs and TiO_2 nanoparticles, improving photogenerated electron transfer. This assembly strategy might dramatically improve photocurrent response and photovoltaic conversion efficiency, being further expanded to photoelectrochemical biosensing.

To date, different from sandwich-type biosensors, few works has referred to the field of photoelectrochemical detection using competitive strategy, which can save diagnosis time, and is cost-effective and potential for on-the-spot diagnosis. Especially, it improves therapeutic outcomes with low cost and decreases patient stress (Hanash et al., 2011), together with less non-specific interferes compared to direct immunosensing. Meanwhile, it can be used to detect not only macromolecules (protein), but also small molecules (drugs, hormones, hapten). In this work, a facile competitive photoelectrochemical determination platform based on the CdSe/TiO_2–RGO nanocomposites films was developed. After adjustment of pH, the positively charged TiO_2–RGO hybrids suspension could assemble with the electronegatively mercaptoacetic acid wrapped CdSe (MPA–CdSe) QDs through electrostatic interaction to form CdSe/TiO_2–RGO nanocomposites films (Jin et al., 2012; Chakrapani et al., 2010). The insoluble and insulating benzo-4-chlorohexadienone (B-4-CHD) produced by biocatalyzed precipitation (BCP), was formed on the biosensor surface (Akter et al., 2012; Zhao et al., 2012a, 2012b). After introducing biological recognition and competitive immunoreaction, a low potential and competitive photoelectrochemical biosensor for carcinoembryonic antigen (CEA) detection was fabricated (Scheme 1). The effects of horseradish peroxide (HRP) impeding the light absorbance and B-4-CHD inhibiting ascorbic acid (AA) diffusion to the electrode surface, functioned as a synergic effect for the decrease of background signal, leading to signal amplification.

2. Experimental

2.1. Reagents and materials

Graphite (99.95%, 8000 mesh) was obtained from Aladdin industrial Corporation. TiO_2 nanopowder (anatase, <25 nm, 99.7%), N-Hydroxysuccinimide (NHS), 1-ethyl-3-(3-(dimethylamino)-propyl) carbodiimide (EDC) and bovine serum albumin (BSA) were obtained from Sigma-Aldrich. 4-chloro-1-naphthol (4-CN) was obtained

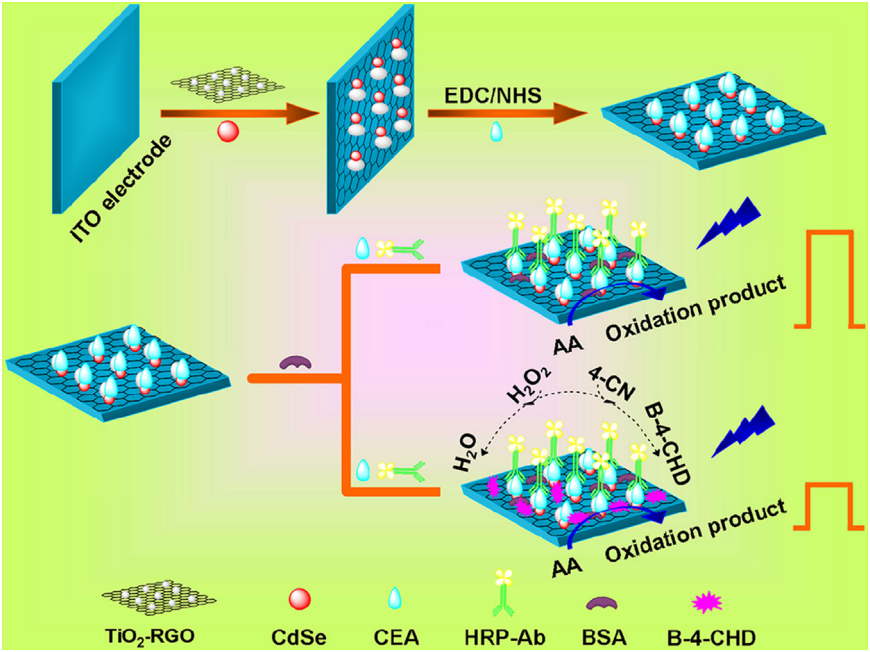

Scheme 1. Schematic illustration of the photoelectrochemical biosensing platform using CdSe QDs and TiO_2 functionalized RGO.

from Tokyo Kasei Kogyo Co., Ltd (Japan). Cadmium chloride ($CdCl_2 \cdot 2.5H_2O$) was purchased from Shanghai Reagent Co., Ltd. (Shanghai, China). Selenium metal powder ($\geq 99.95\%$) was obtained from Shanghai Meixing Chemical Co., Ltd. (Shanghai, China). Mercaptoacetic acid (97%) was purchased from Alfa Aesar China Ltd. Carcinoembryonic antigen (CEA) and horseradish peroxide labeled anti-CEA antibody (HRP-Ab) were purchased from Beijing Keybiotech Co., Ltd (China). Ascorbic acid (AA) and Hydrogen peroxide (H_2O_2) were obtained from Sinopharm Chemical Reagent Co., Ltd (China). Other chemicals were of analytical reagent grade. The washing solution was phosphate buffered saline (PBS) (0.01 mol L^{-1}, pH 7.4). The pH in the tested solution was at 5.5. PBS (0.01 mol L^{-1}, pH 7.4) containing BSA (1%, w/v) was used as blocking solution. Ultrapure water obtained from a Millipore water purification system (≥ 18 MΩ, Milli-Q, Millipore) was used in all assays. Blood samples from Jiangsu Hospital of Cancer were centrifuged at 4000 rpm for 5 min to obtain the supernates as clinical serum samples.

2.2. Apparatus

The photoelectrochemical measurements were performed with a Zahner photoelectrochemical workstation (Universal Analytical and Testing Instruments, Ltd., Germany). All experiments were carried out at room temperature using a conventional three-electrode system with a modified indium tin oxide (ITO) electrode (sheet resistance, 20–25 Ω/sq) with a geometrical area of 1.0 ± 0.1 cm^2 as working, a platinum wire as auxiliary, and a Ag/AgCl electrode as reference electrodes. All of the photocurrent measurements were carried out under 430 nm irradiation at a constant potential of 0 V (*versus* Ag/AgCl) in PBS (0.1 mol L^{-1}, pH 5.5) containing AA (0.1 mol L^{-1}), which was deaerated with high purity nitrogen for 15 min before photoelectrochemical experiments and then kept over a N_2 atmosphere for the entire experimental process. Energy dispersive X-ray analysis spectrum (EDS) was performed in the Field Emission Scanning Electron Microscope (FE-SEM) operating at an accelerating voltage of 20 kV (JEOL, Japan). Electrochemical impedance spectroscopy (EIS) was carried out with an Autolab potentiostat/galvanostat PGSTAT302N (Eco chemie, BV, The Netherlands) and controlled by Nova 1.8 software with a three-electrode system, in KCl solution (0.1 mol L^{-1}) containing a $K_3Fe(CN)_6/K_4Fe(CN)_6$ (5.0 mmol L^{-1}) (1:1) mixture as a redox probe from 0.1 Hz–100 kHz with a signal amplitude of 10 mV. Transmission electrochemical microscope (TEM) images were taken using a Hitachi H-7650 type transmission electron microscope at an accelerating voltage of 80 kV (Hitachi, Japan). Atomic Force microscope (AFM) images were recorded with a Nanoscope IIIa scanning probe microscope (Agilent, USA) using a tapping mode. Ultraviolet–visible (UV–vis) absorption spectra were obtained on Cary 60 spectrophotometer (Agilent, USA). PL spectrum was recorded on Cary Eclipse (Varian, USA). Fourier transform infrared (FTIR) spectra were acquired in the range of 400–4000 cm^{-1} on Tensor 27 (Bruker, Germany) at room temperature. The X-ray diffraction (XRD) patterns were detected on a powder sample using a D/max-RA X-ray diffractometer (Japan) equipped with graphite monochromatized Cu Kα radiation ($\lambda = 1.54056$ Å) in 2θ ranging from 5° to 85° with a scan rate of 1.2 deg min^{-1} at 40 kV and 100 mA, respectively. Raman spectrum measurements were carried out with Labram HR800 microscopic confocal Raman spectrometer (HORIBA Jobin Yvon, France).

2.3. Synthesis of RGO, TiO_2–RGO hybrids, and MPA–CdSe

GO was synthesized by the modified Hummers' method (Kovtyukhova et al., 1999). Then, GO (50 mg) obtained was dispersed in DMF by sonication. After 6 h of stirring, the GO was reduced by hydrazine hydrate (20 mL), followed by washing and centrifugation, RGO was obtained and then dried at 40 °C for further use.

TiO_2–RGO hybrids were adapted from the previous report (Guo and Sun, 2012). Firstly, TiO_2 was calcined in a muffle furnace at 450 °C for 30 min. After being allowed to room temperature, the calcined TiO_2 (8 mg) and the prepared RGO (2 mg) were added to N, N-Dimethylformamide (DMF) (4 mL) and sonication for 4 h. Then ethanol (4 mL) was added, and the suspension was centrifuged at 9500 rpm for 3 min to separate the TiO_2–RGO from the solvents. This process was repeated for 5 times to obtain TiO_2–RGO hybrids. Then, TiO_2–RGO hybrids (4 mg) were added to water (4 mL) to get TiO_2–RGO suspension (1 mg mL^{-1}) and adjusted the pH value of suspension to 5.5.

MPA–CdSe QDs were synthesized according to the previous report with a slight modification (Jiang and Ju, 2007). After deoxygen deionized water (50 ml) containing $CdCl_2$ (2 mmol L^{-1}) was mixed with MPA (20 μL), NaOH solution (1 mol L^{-1}) was added to adjust its pH value to 10.0. The mixture was bubbled with highly pure N_2 for 30 min. Then freshly prepared NaHSe solution (0.7 mL, 0.7 mmol L^{-1}) was injected into the mixture to obtain a clear light yellow MPA–CdSe QDs solution after refluxed at 100 °C for 4 h. After cooling under N_2 atmosphere, the obtained solution was stored at 4 °C before use.

2.4. Preparation of photoelectrochemical biosensor

An ITO electrode was boiled in NaOH solution (2 mol L^{-1}) after successive sonication in acetone, alcohol, and deionized water for 15 min, respectively. Then, the ITO electrode was rinsed with deionized water and allowed to dry at room temperature. TiO_2–RGO hybrids suspension (25 μL, pH 5.5) was dropped on the pretreated ITO sheet. Then, CdSe/TiO_2–RGO nanocomposites films were prepared after the MPA–CdSe solution (25 μL) casting onto the TiO_2–RGO hybrids modified electrode under drying. Thoroughly rising with deionized water, it was activated by immersion in 1.0 mL aqueous solution containing EDC (20 mg) and NHS (10 mg) for 1 h at room temperature, followed by thoroughly rising with washing solution to wash off the excessive EDC and NHS. CEA solution (20 μL, 200 ng mL^{-1}, pH 7.4) was applied to the activated nanocomposites films and incubated at 4 °C for 12 h. Then it was rinsed with washing buffer for removing physically absorbed CEA to obtain a CEA/CdSe/TiO_2–RGO modified ITO electrode. Finally, the CEA/CdSe/TiO_2–RGO modified ITO electrode incubated with BSA (2.5 wt %, 50 μL) at room temperature for 1 h to block nonspecific binding sites. After rinsing with washing solution, the photoelectrochemical biosensor was obtained.

2.5. Photoelectrochemical measurements

CEA solutions (20 μL) with different concentrations were mixed with HRP-Ab (20 μL, 200 ng mL^{-1}) to obtained the incubation solution. Next, incubation solution (20 μL) was dropped onto the photoelectrochemical biosensor and incubated for 60 min at 37 °C. Then it was rinsed carefully with washing solution for removing nonspecifically bonding conjugations to obtain HRP-Ab/BSA/CEA/CdSe/TiO_2–RGO modified ITO electrode. Finally, the modified electrode obtained above was incubated with the PBS consisting of 4-CN (1.0×10^{-3} mol L^{-1}) and H_2O_2 (1.5×10^{-4} mol L^{-1}) for 10 min, to get B-4-CHD on the photoelectrochemical biosensor surface. B-4-CHD was produced from the BCP of 4-CN. Thoroughly rinsing with washing buffer, B-4-CHD/HRP-Ab/BSA/CEA/CdSe/TiO_2–RGO modified ITO electrode was obtained. Then it was inserted in PBS (0.1 mol L^{-1}, pH 5.5) containing AA (0.1 mol L^{-1}) with a bias potential of 0 V at 430 nm irradiation for carrying out photoelectrochemical measurements.

3. Results and discussion

3.1. Characterizations of CdSe/TiO_2–RGO

As shown in atomic force microscopic (AFM) image (Fig. 1A), the thickness of the synthesized RGO sheet was about 1 nm, which was in good agreement with RGO monolayer reported before (Kim et al., 2010), indicating good dispersion of RGO sheet. Transmission electron microscopic (TEM) image was used to further characterize the formation of RGO sheets (Fig. 1B), the RGO sheets were rippled and resembled crumpled silk veil waves, which was suitable for immobilizing nanoparticles. Highly dense deposit of TiO_2 nanoparticles on RGO sheets could be observed (Fig. 1C), which was consistent with Fourier transform infrared (FTIR), Raman and XRD spectra (Fig. S1). The structure was beneficial for photoinduced electron transfer between TiO_2 nanoparticles and RGO.

UV–vis absorption spectra were used to characterize the formation of RGO from the reduction of graphene oxide (GO) sheets (Fig. S2). A bathochromic shift of the absorption peak due to the $\pi \rightarrow \pi^*$ transition of C=C from 230 nm (curve *a*) to 270 nm (curve *b*) was shown, suggesting the formation of RGO from the reduction of GO sheets (Luo et al., 2009), which was consistent with the FTIR spectra (Fig. S1A). The phenomenon also indicated the electronic conjugation within the graphene sheets was restored after the reduction (Li et al., 2008), which could facilitate the photoinduced electron transfer.

UV–vis absorption and photoluminescence (PL) emission spectra of CdSe QDs were displayed in Fig. 2A. UV–vis absorption spectrum showed an obvious peak at 492 nm which corresponded to the first absorption peak of quantum-confined CdSe QDs (curve *a*). The PL spectrum exhibited sharp emission maximum at 521 nm with a full width at half-maximum of about 10 nm (curve *b*), which indicated a narrow size distribution (Jiang and Ju, 2007). Fig. 2B showed the absorption spectra of TiO_2–RGO (curve *a*), and CdSe/TiO_2–RGO nanocomposites before (curve *b*) and after (curve *c*) the pH value was adjusted to 5.5. The absorption spectrum of CdSe/TiO_2–RGO nanocomposites showed a CdSe QDs absorption peak at about 495 nm accompanied by the wide absorption band of TiO_2–RGO, suggesting that CdSe QDs assembled on TiO_2–RGO hybrids. When the pH value of the TiO_2–RGO hybrids suspension was adjusted to 5.5, the absorption of CdSe QDs at about 495 nm enhanced. The reason might be that, after adjustment of pH, the positively charged TiO_2–RGO hybrids suspension assembled on the electronegative MPA–CdSe QDs through electrostatic interactions (Jin et al., 2012) rather than physical absorption, which more amounts of CdSe QDs could assemble on TiO_2–RGO hybrids, leading to the enhancement of absorption at 495 nm. As a two dimensional nanocomposite, the TiO_2–RGO owned a high specific surface area (theoretically 2630 m^2/g for single-layer graphene) (Kim et al., 2010), therefore, CdSe QDs might fully cover the surface of TiO_2–RGO hybrids. According to the reference (Jiang and Ju, 2007), the concentration of CdSe QDs was about 0.05 mmol L^{-1}. Thus, the amount of CdSe QDs assembled on the hybrids was estimated to be 1.25 nmol.

Comparing with energy dispersive X-ray spectroscopy (EDS) spectrum of TiO_2–RGO hybrids (Fig. 2C), the EDS spectrum of CdSe/TiO_2–RGO nanocomposites showed Cd, Se and S elements peaks apart from C, O, and Ti elements peaks (Fig. 2D). This phenomenon verified that CdSe QDs successfully assembled on TiO_2–RGO hybrids, which was consistent with the UV–vis absorption spectrum (curve *c*, Fig. 2B).

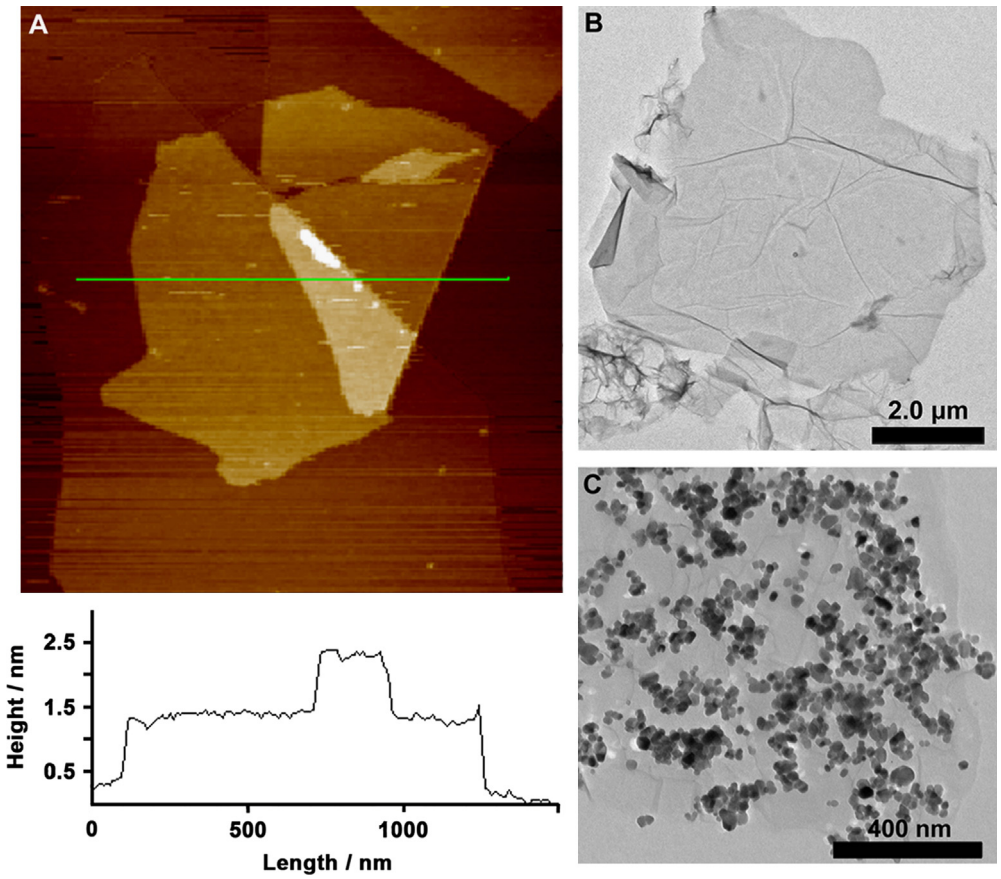

Fig. 1. The AFM image of RGO (A), and the TEM images of RGO (B) and TiO_2–RGO (C).

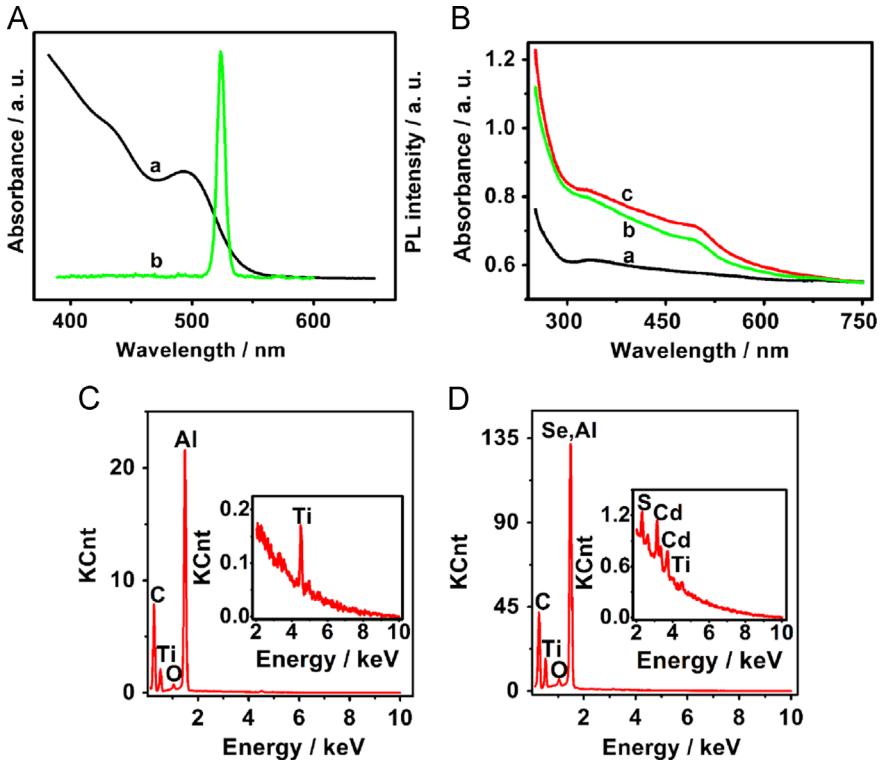

Fig. 2. (A) UV–vis absorption (a) and fluorescence spectra (b) of CdSe QDs with excitation wavelength at 380 nm. (B) UV–vis absorption spectra of TiO_2–RGO (a), CdSe/TiO_2–RGO before (b) and after (c) the pH value of TiO_2–RGO suspension was adjusted to 5.5. The EDS spectra of (C) TiO_2–RGO and (D) CdSe/TiO_2–RGO. Inset: magnified response.

3.2. Photoeletrochemical response of CdSe/TiO_2–RGO

The photoelectrochemical responses of TiO_2, TiO_2–RGO and CdSe/TiO_2–RGO modified ITO electrodes were investigated in PBS (0.1 mol L^{-1}, pH 7.4) containing AA (0.1 mol L^{-1}) (Fig. 3A). Compared to the photocurrent of TiO_2 modified ITO electrode (curve *a*), the photocurrent of TiO_2–RGO modified ITO electrode (curve *b*) increased 39.0%, which was attributed to the good conductivity of RGO, accelerating the photoinduced electron transfer. Based on the large surface area of TiO_2–RGO hybrids, large amounts of CdSe QDs were immobilized. The photocurrent of CdSe/TiO_2–RGO modified ITO electrode (curve *c*) further improved and increased to 1.77 μA. CdSe QDs with narrow band gap could be easier excited by visible light of the same intensity, leading to charge separation to yield electrons and holes. While the holes were scavenged by AA, which was an electron donor, the electrons were collected by the ITO electrode through TiO_2–RGO hybrids, hence enhancing photocurrent and overall photovoltaic conversion efficiency. After the pH value of TiO_2–RGO suspension was adjusted to 5.5, the photocurrent (16.8 μA) obviously improved and enhanced nearly 8.5 times (curve *d*), comparing with that of TiO_2–RGO suspension (pH 7.4) with assembling CdSe QDs modified ITO electrode (curve *c*). The dramatic enhancement of the photocurrent might be attributed to two aspects. On one hand, after the pH value of the TiO_2–RGO suspension was adjusted to 5.5, the positively charged TiO_2–RGO hybrids suspension could assemble on the MPA–CdSe QDs through electrostatic interaction to form CdSe/TiO_2–RGO nanocomposites films rather than physical absorption, leading to increase the amount of CdSe QDs immobilized (Jin et al., 2012).

On the other hand, after acid treatment, pH-induced protonation of surface groups on TiO_2 tuned the band edge of TiO_2, and it generated a energy gap for facilitating charge injection between excited CdSe and TiO_2 (Chakrapani et al., 2010), improving photogenerated electron transfer and photovoltaic conversion efficiency. As seen, after 5 on-off cycles, the photocurrent response of CdSe/TiO_2–RGO modified ITO electrode was stable, only 3.6% alteration to the initial photocurrent response (Fig. 3B). Moreover, the photocurrent could be turned on and off by controlling the light. Based on the high photovoltaic conversion efficiency and good stability of CdSe/TiO_2–RGO nanocomposites films, it was advantageously used for developing photoelectrochemical determination platform.

3.3. Characterizing the fabrication process of photoelectrochemical biosensor

As shown in Fig. 3C, the stepwise assembly process of the photoelectrochemical biosensor was investigated by the electrochemical impedance spectroscopy (EIS). After the CdSe/TiO_2–RGO nanocomposites films were coated onto ITO, the impedance spectrum exhibited a small semicircle (curve *a*), suggesting that RGO accelerated the electron transfer between the redox probe and electrode surface due to its excellent electronic conductivity. Subsequently, CEA covalently bond to the CdSe/TiO_2–RGO nanocomposites films, leading to an increase of R_{et} (curve *b*). After bovine serum albumin (BSA) blocking and subsequent stepwise immobilization of HRP-Ab and B-4-CHD, the R_{et} increased gradually (curves *c*–*e*), indicating the successful assembly of HRP-Ab and the formation of B-4-CHD on the electrode surface. The increase of electron transfer resistance verified the successful fabrication of the photoelectrochemical biosensor.

Meanwhile, the photoelectrochemical response at each immobilization step was recorded to further monitor the fabrication of the biosensor (Fig. 3D). A large photocurrent (16.8 μA) was observed (curve *a*) at the CdSe/TiO_2–RGO nanocomposites films modified ITO electrode, which was attributed to the high photovoltaic conversion efficiency of CdSe/TiO_2–RGO nanocomposites films and the good conductivity of RGO, accelerating the photoinduced electron transfer. The photocurrents decreased sharply with the immobilization of CEA (curve *b*) and further decreased

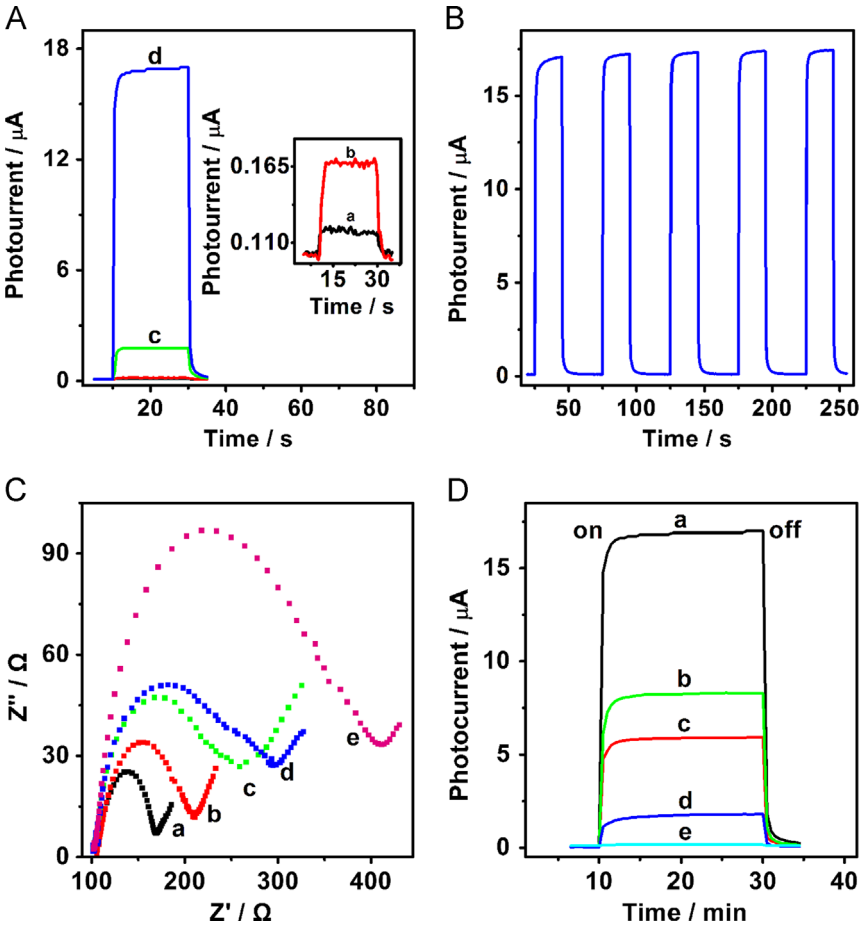

Fig. 3. (A) The photoelectrochemical responses of TiO_2 (a), TiO_2–RGO (b), and CdSe/TiO_2–RGO before (c) and after the pH value of TiO_2–RGO suspension was adjusted to 5.5 (d) modified ITO electrodes. Inset: magnified photoelectrochemical responses of (a) and (b). (B) The photoelectrochemical response of CdSe/TiO_2–RGO modified ITO electrode. The EIS (C) and the photocurrent responses (D) of CdSe/TiO_2–RGO (a), CEA/CdSe/TiO_2–RGO (b), BSA/CEA/CdSe/TiO_2–RGO (c), HRP-Ab/BSA/CEA/CdSe/TiO_2–RGO (d), B-4-CHD/HRP-Ab/BSA/CEA/CdSe/TiO_2–RGO (e) modified ITO electrodes in the incubation solution containing 10.0 ng mL^{-1} CEA.

after BSA blocking (curve *c*), only 48.4% and 34.6% of that obtained from the CdSe/TiO_2–RGO nanocomposites films modified ITO, respectively, which was due to the steric hindrance of the hydrophobic protein layer that impeded the AA diffusion to the electrode surface for scavenging the holes. In addition, the protein layer immobilized on the electrode might block photogenerated electron transfer. Followed by the conjugation of HRP-Ab (curve *d*) and incubation with BCP solution (curve *e*), the photocurrent continued to decrease to 10.1% and 1.0% of that obtained from the CdSe/TiO_2–RGO nanocomposites films modified ITO, respectively. The strong light-harvesting property of HRP at around 430 nm would intercept the irradiation light. HRP produced a competitive non-productive absorption that lowered the irradiation intensity on the photoelectrochemical biosensor, thus hampering the photocurrent generation (Tang and Ren, 2008; Chen et al., 2010; Zhao et al., 2012a, 2012b). Besides, 4-chloro-1-naphthol (4-CN) was oxidized by H_2O_2 with the assistance of HRP to produce B-4-CHD in BCP solution. B-4-CHD absorbed on RGO via π–π conjugation, which led to hinder the AA diffusion to the electrode surface for scavenging the holes (Zhao et al., 2012a, 2012b; Zhang et al., 2010). The synergic effect of HRP and B-4-CHD reduced the background signal of photoelectrochemical determination for signal amplification.

3.4. Photoelectrochemical biosensing for CEA

Under the optimal conditions (Figs. S3–S5), the photocurrent responses measured by varying the CEA concentration were revealed in Fig. 4A. As show in the plot, photocurrents increased with the increase of the concentration of the CEA (*C*). The calibration plot was constructed by plotting ΔI ($\Delta I = I - I_0$, I was the photocurrent of CEA solutions with different concentrations and I_0 was the bank photocurrent.) against CEA concentrations in a linear range from 0.003 to 100 ng mL^{-1} (Fig. 4B). The correlation coefficient was 0.999 and the detection limit was estimated to be 1.38 pg mL^{-1} at a *S*/*N* of 3. The linear range (0.003–100 ng mL^{-1}) was much wider than 1.0–60 ng mL^{-1} by the CL method (Yang et al., 2009) and 0.04–80 ng mL^{-1} by electrochemical method (Zhuo et al., 2009). The detection limit of 1.38 pg mL^{-1} was lower than 20 ng mL^{-1} by SPR immunoassay (Hu et al., 2010) and 0.5 ng mL^{-1} by ECL immunoassay (Ge et al., 2012). In addition, the detection potential was more close to physiological potential than −0.84 V by the electrochemical method (Ho et al., 2009) and −1.49 V by the ECL method (Jie et al., 2010), leading to less interference.

3.5. Reproducibility, stability and specificity of the photoelectrochemical biosensor

Both the intra-assay and interassay precision of the photoelectrochemical biosensor were examined. The relative standard deviations (RSD) of intra-assay were 4.1%, 4.8% and 4.2% at 0.5, 10, and 100 ng ml^{-1}, respectively, whereas the interassay RSD of 5.7%, 6.1%, and 4.9% were obtained by measuring the same samples with four electrodes prepared independently at the identical experimental conditions, which showed good precision and acceptable

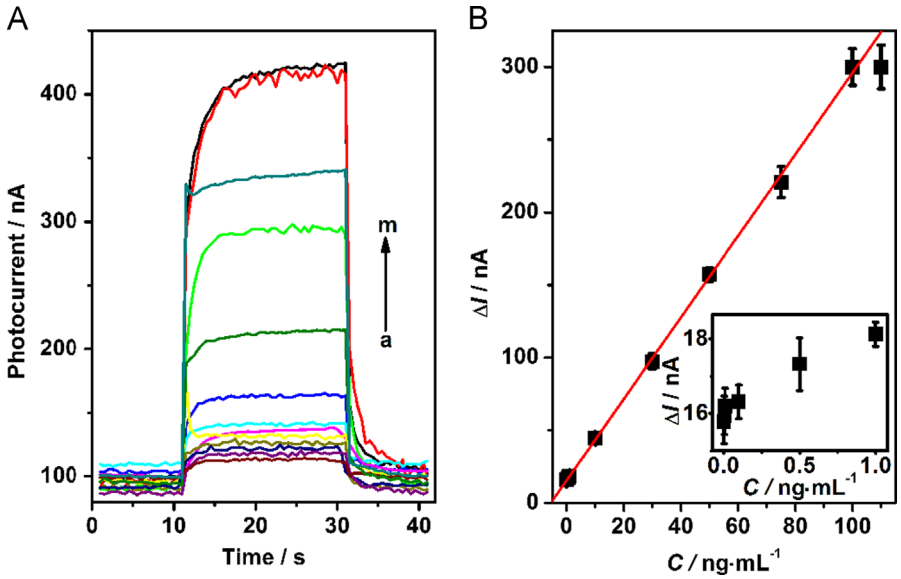

Fig. 4. (A) Photoelectrochemical responses of the biosensor to (a–m) 0, 0.003, 0.005, 0.01, 0.1, 0.5, 1, 10, 30, 50, 75, 100, 110 ng mL^{-1} CEA, and (B) linear calibration curve. Inset: magnified responses from 0.003 to 1 ng mL^{-1} for CEA determination.

fabrication reproducibility. In addition, for the detection of 10 ng mL^{-1} CEA, the photocurrent showed nearly no change after 10 repeated measurements, indicating the stable readout for signal collection. When the photoelectrochemical biosensor was stored in shade at 4 °C before it was used for further measurement, it retained 90.7% of its initial response after ten days, indicating good long-term stability. In addition, the photoelectrochemical biosensor exhibited an excellent specificity for the detection of CEA (Fig. S5).

3.6. Detection of CEA in clinical serum samples

This photoelectrochemical biosensor could be used for clinical sample detection. When the level of serum tumor marker was over the calibration range, serum sample was appropriately diluted with 0.01 mol L^{-1} pH 7.4 PBS prior to assay. The assay results of clinical serum samples, compared with the reference values obtained by commercial turbidimetric immunoassay, showed an acceptable agreement, with relative deviation less than 11.2% (Table 1), indicating acceptable accuracy of the proposed photoelectrochemical biosensor for clinical samples detections.

Table 1
Comparison of serum CEA levels determination using the reference and proposed methods.

Sample	S6	S5	S4	S3	S2	S1
Reference method [ng ml^{-1}]	26.445	12.195	5.285	2.41	1.265	1.388
Proposed method [ng ml^{-1}][a]	27.508	11.386	4.909	2.68	1.388	0.815
Relative deviation [%]	4.02	−6.6	−7.11	11.20	9.72	6.54

[a] Average value from three successive determinations.

4. Conclusions

A low potential and competitive photoelectrochemical biosensing platform based on the CdSe/TiO_2–RGO nanocomposites films was developed. After adjustment of pH, the positively charged TiO_2–RGO hybrids suspension could assemble with the electronegatively MPA–CdSe QDs through electrostatic interaction to form CdSe/TiO_2–RGO nanocomposites films. CdSe/TiO_2–RGO nanocomposites films exhibited high photovoltaic conversion efficiency and good stability under irradiation of visible light at 0 V. By combining with biological recognition and competitive immunoreaction, a facile competitive photoelectrochemical biosensing platform based on the CdSe/TiO_2–RGO nanocomposites films for CEA detection was developed. The effects of HRP impeding the light absorbance and B-4-CHD inhibiting AA diffusion to the electrode surface, functioned as a synergic effect for the decrease of background signal, leading to signal amplification. The proposed competitive photoelectrochemical biosensor under irradiation of visible light exhibited excellent performance, such as low potential, wide linear range, low detection limit, good reproducibility, excellent specificity, and it was satisfactory for clinical sample detection. Since QDs sensitized TiO_2–RGO functional films owned high photovoltaic conversion efficiency, the designed strategy has an expansive and promising perspective of application in other biological recognition and tumor markers detection for constructing versatile photoelectrochemical biosensing platforms.

Acknowledgments

This work was supported by the National Natural Science Foundation of China for the project (21175069 and 21205061), Natural Science Foundation of Jiangsu (BK2012448) and Foundation of the Jiangsu Education Committee (11KJA150003). We appreciate the financial support from the Priority Academic Program Development of Jiangsu Higher Education Institutions and the Program for Jiangsu Collaborative Innovation Center of Biomedical Functional Materials.

Appendix. Supplementary material

Supplementary data associated with this article can be found in the online version at http://dx.doi.org/10.1016/j.bios.2013.10.057.

References

Akter, R., Rahman, M.A., Rhee, C.K., 2012. Anal. Chem. 84, 6407–6415.
Cai, J., Sheng, P.T., Zhou, L.P., Wang, N.Y., Cai, Q.Y., 2013. Biosens. Bioelectron. 50, 66–71.
Chakrapani, V., Tvrdy, K., Kamat, P.V., 2010. J. Am. Chem. Soc. 132, 1228–1229.
Chen, D., Zhang, H., Li, X., Li, J.H., 2010. Anal. Chem. 82, 2253–2261.

Chikkaveeraiah, B.V., Bhirde, A.A., Morgan, N.Y., Eden, H.S., Chen, X.Y., 2012. ACS Nano 6, 6546–6561.
Choi, S., Jin, H., Bang, J., Kim, S., 2012. J. Phys. Chem. Lett. 3, 3442–3447.
Ge, L., Yan, J.X., Song, X.R., Yan, M., Ge, S.G., Yu, J.H., 2012. Biomaterials 33, 1024–1031.
Gill, R., Zayats, M., Willner, I., 2008. Angew. Chem. Int. Ed. 47, 7602–7625.
Guo, S.J., Sun, S.H., 2012. J. Am. Chem. Soc. 134, 2492–2495.
Hanash, S.M., Baik, C.S., Kallioniemi, O., 2011. Nat. Rev. Clin. Oncol. 8, 142–150.
Hensel, J., Wang, G.M., Li, Y., Zhang, J.Z., 2010. Nano Lett. 10, 478–483.
Ho, J.A.A., Lin, Y.C., Wang, L.S., Hwang, K.C., Chou, P.T., 2009. Anal. Chem. 81, 1340–1346.
Huang, Q.L., Chen, H., Xu, L.L., Lu, D.Q., Tang, L.L., Jin, L.T., Xu, Z.A., Zhang, W., 2013. Biosens. Bioelectron. 45, 292–299.
Hu, W.H., Liu, Y.S., Lu, Z.S., Li, C.M., 2010. Adv. Funct. Mater. 20, 3497–3503.
Ikeda, A., Nakasu, M., Ogasawara, S., Nakanishi, H., Nakamura, M., Kikuchi, J., 2009. Org. Lett. 11, 1163–1166.
Jiang, H., Ju, H.X., 2007. Anal. Chem. 79, 6690–6696.
Jie, G.F., Liu, P., Zhang, S.S., 2010. Chem. Commun. 46, 1323–1325.
Jin, H., Choi, S., Velu, R., Kim, S., Lee, H.J., 2012. Langmuir 28, 5417–5426.
Kim, T., Lee, H., Kim, J., Suh, K.S., 2010. ACS Nano 4, 1612–1618.
Kovtyukhova, N.I., Ollivier, P.J., Martin, B.R., Mallouk, T.E., Chizhik, S.A., Buzaneva, E.V., Gorchinskiy, A.D., 1999. Chem. Mater. 11, 771–778.
Kulasingam, V., Diamandis, E.P., 2008. Nat. Clin. Pract. Oncol. 5, 588–599.
Lee, J.S., You, K.H., Park, C.B., 2012. Adv. Mater. 24, 1084–1088.
Li, D., Mueller, M.B., Gilje, S., Kaner, R.B., Wallace, G.G., 2008. Nat. Nanotechnol. 3, 101–105.
Li, L.L., Liu, K.P., Yang, G.H., Wang, C.M., Zhang, J.R., Zhu, J.J., 2011a. Adv. Funct. Mater. 21, 869–878.
Li, Y.J., Ma, M.J., Zhu, J.J., 2012. Anal. Chem. 84, 10492–10499.
Li, N., Liu, G., Zhen, C., Li, F., Zhang, L.L., Cheng, H.M., 2011b. Adv. Funct. Mater. 21, 1717–1722.
Long, R., English, N.J., Prezhdo, O.V., 2012. J. Am. Chem. Soc. 134, 14238–14248.
Luo, Z.T., Lu, Y., Somers, L.A., Johnson, A.T.C., 2009. J. Am. Chem. Soc. 131, 898–899.
Munge, B.S., Coffey, A.L., Doucette, J.M., Somba, B.K., Malhotra, R., Patel, V., Gutkind, J.S., Rusling, J.F., 2011. Angew. Chem. Int. Ed. 50, 7915–7918.
Nie, H.G., Liu, S.J., Yu, R.Q., Jiang, J.H., 2009. Angew. Chem. Int. Ed. 48, 9862–9866.
Ocvirk, R., Franklin, K.B.J., Murphy, B.E.P., 2009. Anal. Chem. 81, 1191–1197.
Schaefer, O., Bohlmann, R., Schleuning, W.D., Schulze-Forster, K., Hümpel, M., 2005. J. Agric. Food Chem. 53, 2881–2889.
Tang, D.P., Ren, J.J., 2008. Anal. Chem. 80, 8064–8070.
Tang, Y.B., Lee, C.S., Xu, J., Liu, Z.T., Chen, Z.H., He, Z.B., Cao, Y.L., Yuan, G.D., Song, H.S., Chen, L.M., Luo, L.B., Cheng, H.M., Zhang, W.J., Bello, I., Lee, S.T., 2010. ACS Nano 4, 3482–3488.
Tu, W.W., Wang, W.J., Lei, J.P., Deng, S.Y., Ju, H.X., 2012. Chem. Commun. 48, 6535–6537.
Tvrdy, K., Frantsuzov, P.A., Kamat, P.V., 2011. Proc. Nat. Acad. Sci. USA. 108, 113–117.
Wang, G.L., Xu, J.J., Chen, H.Y., Fu, S.Z., 2009. Biosens. Bioelectron. 25, 791–796.
Yang, Z.J., Liu, H., Zong, C., Yan, F., Ju, H.X., 2009. Anal. Chem. 81, 5484–5489.
Zhao, L.J., Hu, L.F., Fang, X.S., 2012a. Adv. Funct. Mater. 22, 1551–1566.
Zhao, W.W., Dong, X.Y., Wang, J., Kong, F.Y., Xu, J.J., Chen, H.Y., 2012b. Chem. Commun. 48, 5253–5255.
Zhang, B., Zhang, X., Yan, H.H., Xu, S.J., Tang, D.H., Fu, W.L., 2007. Biosens. Bioelectron. 23, 19–25.
Zhang, H., Lv, X.J., Li, Y.M., Wang, Y., Li, J.H., 2010. ACS Nano 4, 380–386.
Zhang, X.R., Li, S.G., Jin, X., Li, X.M., 2011. Biosens. Bioelectron. 47, 4929–4931.
Zhuo, Y., Yuan, P.X., Yuan, R., Chai, Y.Q., Hong, C.L., 2009. Biomaterials 30, 2284–2290.